

Understanding Training-free Diffusion Guidance: Mechanisms and Limitations

Yifei Shen¹, Xinyang Jiang¹, Yezhen Wang², Yifan Yang¹, Dongqi Han¹, and Dongsheng Li¹

¹ Microsoft Research Asia

{yifeishen,xinyangjiang,yifanyang,dongqihan,dongsheng.li}@microsoft.com

² National University of Singapore

yezhen.wang0305@gmail.com

Abstract. Adding additional control to pretrained diffusion models has become an increasingly popular research area, with extensive applications in computer vision, reinforcement learning, and AI for science. Recently, several studies have proposed training-free diffusion guidance by using off-the-shelf networks pretrained on clean images. This approach enables zero-shot conditional generation for universal control formats, which appears to offer a free lunch in diffusion guidance. In this paper, we aim to develop a deeper understanding of the operational mechanisms and fundamental limitations of training-free guidance. We offer a theoretical analysis that supports training-free guidance from the perspective of optimization, distinguishing it from classifier-based (or classifier-free) guidance. To elucidate their drawbacks, we theoretically demonstrate that training-free methods are more susceptible to adversarial gradients and exhibit slower convergence rates compared to classifier guidance. We then introduce a collection of techniques designed to overcome the limitations, accompanied by theoretical rationale and empirical evidence. Our experiments in image and motion generation confirm the efficacy of these techniques.

1 Introduction

1.1 Motivations

Diffusion models represent a class of powerful deep generative models that have recently broken the long-standing dominance of generative adversarial networks (GANs) [7]. These models have demonstrated remarkable success in a variety of domains, including the generation of images and videos in computer vision [3, 29], the synthesis of molecules and proteins in computational biology [16, 47], as well as the creation of trajectories and actions in the field of reinforcement learning (RL) [17].

One critical area of research in the field of diffusion models involves enhancing controllability, such as pose manipulation in image diffusion [45], modulation of quantum properties in molecule diffusion [16], and direction of goal-oriented actions in RL diffusion [19]. The predominant techniques for exerting control over

diffusion models include classifier guidance and classifier-free guidance. Classifier guidance involves training a time-dependent classifier to map a noisy image, denoted as \mathbf{x}_t , to a specific condition \mathbf{y} , and then employing the classifier’s gradient to influence each step of the diffusion process [7]. Conversely, classifier-free guidance bypasses the need for a classifier by training an additional diffusion model conditioned on \mathbf{y} [15]. However, both approaches necessitate extra training to integrate the conditions. Moreover, their efficacy is often constrained when the data-condition pairs are limited and typically lacks the capability for zero-shot generalization to novel conditions.

Recently, several studies [2, 33, 44] have introduced training-free guidance that builds upon the concept of classifier guidance. These models eschew the need for training a classifier on noisy images; instead, they estimate the clean image from its noisy counterpart using Tweedie’s formula and then employ pre-trained networks, designed for clean images, to guide the diffusion process. Given that checkpoints for these networks pretrained on clean images are widely accessible online, this form of guidance can be executed in a zero-shot manner. A unique advantage of training-free guidance is that it can be applied to universal control formats, such as style, layout, and FaceID [2, 33, 44] without any additional training efforts. Furthermore, these algorithms have been successfully applied to offline reinforcement learning, enabling agents to achieve novel goals not previously encountered during training [40]. Despite the encouraging empirical results, the fundamental principles contributing to the success of these methods have yet to be fully elucidated. From a theoretical perspective, it is intriguing to understand how and when these methods succeed or fail. From an empirical standpoint, it is crucial to develop algorithms that can address and overcome these limitations.

This paper seeks to deepen the understanding of training-free guidance by examining its operational mechanisms and inherent limitations. From an optimization standpoint, we demonstrate that training-free guidance has a two-stage convergence, where the second stage enjoys a linear convergence. This is a distinctive feature that is not shared by classifier guidance or classifier-free guidance methods. However, we identify and provide proof that training-free guidance is prone to adversarial gradient issues and slower convergence rates due to the diminished smoothness of the guidance network, when compared to classifier guidance. To address these challenges, we introduce a suite of techniques that have been theoretically and empirically validated for their efficacy. Specifically, our major contributions can be summarized as follows:

- **Mechanisms (How it works):** We offer theoretical proof, from an optimization perspective, that training-free guidance is guaranteed to minimize the loss of the guidance network. This characteristic distinguishes them from approaches that rely on training-based guidance.
- **Limitations (When it does not work):** We theoretically identify the susceptibility of training-free guidance to adversarial gradient issues and slower convergence rates. We attribute these challenges to a decrease in the smoothness of the guidance network in contrast to the classifier guidance.

- **Addressing the limitations:** We introduce a set of enhancement techniques aimed at mitigating the identified limitations. The efficacy of these methods is empirically confirmed across various diffusion models (e.g., image diffusion and motion diffusion) and under multiple conditions (e.g., segmentation, sketch, text, and object avoidance). The code is available at <https://github.com/BIGKnight/Understanding-Training-free-Diffusion-Guidance>.

For more related fields and the impact of this paper in these fields, please refer to Appendix 7.

2 Preliminaries

2.1 Diffusion Models

Diffusion models are characterized by forward and reverse processes. The forward process, occurring over a time interval from 0 to T , incrementally transforms an image into Gaussian noise. On the contrary, the reverse process, from T back to 0, reconstructs the image from the noise. Let \mathbf{x}_t represent the state of the data point at time t ; the forward process systematically introduces noise to the data by following a predefined noise schedule given by

$$\mathbf{x}_t = \sqrt{\alpha_t} \mathbf{x}_0 + \sigma_t \boldsymbol{\epsilon}_t,$$

where $\alpha_t \in [0, 1]$ is monotonically decreasing with t , $\sigma_t = \sqrt{1 - \alpha_t}$, and $\boldsymbol{\epsilon}_t \sim \mathcal{N}(0, \mathbf{I})$ is random noise. Diffusion models use a neural network to learn the noise at each step:

$$\min_{\theta} \mathbb{E}_{\mathbf{x}_t, \boldsymbol{\epsilon}_t} [\|\boldsymbol{\epsilon}_{\theta}(\mathbf{x}_t, t) - \boldsymbol{\epsilon}_t\|_2^2] = \min_{\theta} \mathbb{E}_{\mathbf{x}_t, \boldsymbol{\epsilon}_t} [\|\boldsymbol{\epsilon}_{\theta}(\mathbf{x}_t, t) + \sigma_t \nabla_{\mathbf{x}_t} \log p_t(\mathbf{x}_t)\|_2^2],$$

where $p_t(\mathbf{x}_t)$ is the distribution of \mathbf{x}_t . The reverse process is obtained by the following ODE:

$$\frac{d\mathbf{x}_t}{dt} = f(t)\mathbf{x}_t - \frac{g^2(t)}{2} \nabla_{\mathbf{x}_t} \log p_t(\mathbf{x}_t) = f(t)\mathbf{x}_t + \frac{g^2(t)}{2\sigma_t} \boldsymbol{\epsilon}_{\theta}(\mathbf{x}_t, t), \quad (1)$$

where $f(t) = \frac{d \log \sqrt{\alpha_t}}{dt}$, $g^2(t) = \frac{d\sigma_t^2}{dt} - 2 \frac{d \log \sqrt{\alpha_t}}{dt} \sigma_t^2$. The reverse process enables generation as it converts a Gaussian noise into the image.

2.2 Training-Free Diffusion Guidance

In diffusion control, we aim to sample \mathbf{x}_0 given a condition \mathbf{y} . The conditional score function is expressed as follows:

$$\nabla_{\mathbf{x}_t} \log p_t(\mathbf{x}_t | \mathbf{y}) = \nabla_{\mathbf{x}_t} \log p_t(\mathbf{x}_t) + \nabla_{\mathbf{x}_t} \log p_t(\mathbf{y} | \mathbf{x}_t). \quad (2)$$

The conditions are specified by the output of a neural network, and the energy is quantified by the corresponding loss function. If $\ell(f_{\phi}(\cdot), \cdot)$ represents the loss

function as computed by neural networks, then the distribution of the clean data is expected to follow the following formula [2, 33, 44]:

$$p_0(\mathbf{x}_0|\mathbf{y}) \propto p_0(\mathbf{x}_0) \exp(-\ell(f_\phi(\mathbf{x}_0), \mathbf{y})). \quad (3)$$

For instance, consider a scenario where the condition is the object location. In this case, f_ϕ represents a fastRCNN architecture, and ℓ denotes the classification loss and bounding box loss. By following the computations outlined in [22], we can derive the exact formula for the second term in the RHS of (2) as:

$$\nabla_{\mathbf{x}_t} \log p_t(\mathbf{y}|\mathbf{x}_t) = \nabla_{\mathbf{x}_t} \log \mathbb{E}_{p(\mathbf{x}_0|\mathbf{x}_t)}[\exp(-\ell(f_\phi(\mathbf{x}_0), \mathbf{y}))]. \quad (4)$$

Classifier guidance [7] involves initially training a time-dependent classifier to predict the output of the clean image \mathbf{x}_0 based on noisy intermediate representations \mathbf{x}_t during the diffusion process, i.e., to train a time-dependent classifier $f_\psi(\mathbf{x}_t, t)$ such that $f_\psi(\mathbf{x}_t, t) \approx f_\phi(\mathbf{x}_0)$. Then the gradient of the time-dependent classifier is used for guidance, given by $\nabla_{\mathbf{x}_t} \log p_t(\mathbf{y}|\mathbf{x}_t) := -\nabla_{\mathbf{x}_t} \ell(f_\psi(\mathbf{x}_t, t), \mathbf{y})$.

Classifier guidance corresponds to the energy function in (4) when the loss function employed is cross-entropy. This direct relationship does not hold when alternative loss functions, such as the ℓ_2 distance [22], are utilized. Nonetheless, empirical research [20] indicates that classifier guidance remains effective across a diverse array of applications, including but not limited to text guidance and image similarity guidance.

Training-free guidance [2, 6, 44] puts the expectation in (4) inside the loss function:

$$\begin{aligned} \nabla_{\mathbf{x}_t} \log p_t(\mathbf{y}|\mathbf{x}_t) &:= \nabla_{\mathbf{x}_t} \log [\exp(-\ell(f_\phi(\mathbb{E}_{p(\mathbf{x}_0|\mathbf{x}_t)}(\mathbf{x}_0)), \mathbf{y}))] \\ &\stackrel{(a)}{=} -\nabla_{\mathbf{x}_t} \ell \left[f_\phi \left(\frac{\mathbf{x}_t - \sigma_t \boldsymbol{\epsilon}_\theta(\mathbf{x}_t, t)}{\sqrt{\alpha_t}} \right), \mathbf{y} \right], \end{aligned} \quad (5)$$

where (a) uses Tweedie’s formula $\mathbb{E}_{p(\mathbf{x}_0|\mathbf{x}_t)}(\mathbf{x}_0) = \frac{\mathbf{x}_t - \sigma_t \boldsymbol{\epsilon}_\theta(\mathbf{x}_t, t)}{\sqrt{\alpha_t}}$. Leveraging this approximation permits the use of a pre-trained off-the-shelf network designed for processing clean data. The gradient of the last term in the energy function is obtained via backpropagation through both the guidance network and the diffusion backbone.

3 Analysis of Training-Free Guidance

3.1 Mechanisms of Training-free Guidance

The difficulty of approximating $p_t(\mathbf{y}|\mathbf{x}_t)$ in high-dimensions. From a probabilistic standpoint, it is observed that [33]

$$\begin{aligned} \nabla_{\mathbf{x}_t} \log \mathbb{E}_{p(\mathbf{x}_0|\mathbf{x}_t)}[\exp(-\ell(f_\phi(\mathbf{x}_0), \mathbf{y}))] &\stackrel{(a)}{\approx} \nabla_{\mathbf{x}_t} \log \mathbb{E}_{q(\mathbf{x}_0|\mathbf{x}_t)}[\exp(-\ell(f_\phi(\mathbf{x}_0), \mathbf{y}))] \\ &\approx \nabla_{\mathbf{x}_t} \log \frac{1}{n} \sum_{i=1}^n \exp(-\ell(f_\phi(\mathbf{x}_0^i), \mathbf{y})), \quad \mathbf{x}_0^i \sim q(\mathbf{x}_0|\mathbf{x}_t), \end{aligned} \quad (6)$$

where $q(\mathbf{x}_0|\mathbf{x}_t) = \mathcal{N}(\mathbb{E}_{p(\mathbf{x}_0|\mathbf{x}_t)}(\mathbf{x}_0), r_t^2 \mathbf{I})$ and r_t is a tunable parameter [33]. By taking $n = 1$ and $r_t = 0$, (6) is reduced to the guidance term in (5). As demonstrated in [33], the approximation is effective for one-dimensional distribution. However, the approximation denoted by (a) does not extend to high-dimensional data, such as images. This is due to the well-known high-dimensional probability phenomenon where $q(\mathbf{x}_0|\mathbf{x}_t)$ tends to concentrate on a spherical shell centered at $\mathbb{E}_{p(\mathbf{x}_0|\mathbf{x}_t)}(\mathbf{x}_0)$ with radius r_t , as discussed in Chapter 3.1 of [39]. Since the spherical shell represents a low-dimensional manifold with zero measure in the high-dimensional space, there is a significant likelihood that the supports of $p(\mathbf{x}_0|\mathbf{x}_t)$ and $q(\mathbf{x}_0|\mathbf{x}_t)$ do not overlap, rendering the approximation (a) ineffective.

Training-free guidance minimizes the loss from an optimization perspective. Given the difficulty of analyzing the training-free guidance from a probability perspective, we turn to an optimization perspective for clarity. Denote $\hat{\mathbf{x}}_0 = \mathbb{E}_{p(\mathbf{x}_0|\mathbf{x}_t)}(\mathbf{x}_0)$, the gradient guidance term in (5) can be written as the following:

$$\nabla_{\mathbf{x}_t} \ell[f_\phi(\hat{\mathbf{x}}_0), \mathbf{y}] = \frac{\partial \ell}{\partial \hat{\mathbf{x}}_0} \nabla_{\mathbf{x}_t} \left(\frac{\mathbf{x}_t + \sigma_t^2 \nabla_{\mathbf{x}_t} \log p_t(\mathbf{x}_t)}{\sqrt{\alpha_t}} \right) = \frac{\partial \ell}{\partial \hat{\mathbf{x}}_0} \frac{\text{Cov}[\mathbf{x}_0|\mathbf{x}_t]}{\sigma_t^2 \sqrt{\alpha_t}}, \quad (7)$$

where the last equality follows the second-order Miyasawa relationship $\text{Cov}[\mathbf{x}_0|\mathbf{x}_t] = \sigma_t^2(\mathbf{I} + \sigma_t^2 \nabla^2 \log p_t(\mathbf{x}_t))$ [26]. Based on (7), we show that the guidance steps decrease the loss function associated with the clean classifier f_ϕ , which is shown in the next proposition.

Proposition 1. *Assume that the guidance loss function $\ell(f_\phi(\mathbf{x}_0), \mathbf{y})$ is μ -PL (defined in Definition 2 in appendix) and L_f -Lipschitz with respect to clean images \mathbf{x}_0 , and the score function $\nabla \log p_t(\mathbf{x}_t)$ is L_p -Lipschitz (defined in Definition 1 in appendix) with respect to noisy image \mathbf{x}_t . Then the following conditions hold:*

1. *The loss function $\ell_t(\mathbf{x}_t) = \ell\left(f_\phi\left(\frac{\mathbf{x}_t + \sigma_t^2 \nabla \log p_t(\mathbf{x}_t)}{\sqrt{\alpha_t}}\right), \mathbf{y}\right)$ is $\frac{L_f(1+L_p)}{\sqrt{\alpha_t}}$ -Lipschitz and $\frac{\mu \lambda_{\min}^2}{\sigma_t^4 \alpha_t}$ -PL with respect to the noisy image \mathbf{x}_t , where λ_{\min}^2 is the minimum eigenvalue of positive (semi)-definite matrix $\text{Cov}[\mathbf{x}_0|\mathbf{x}_t]$;*
2. *Denote $\kappa_1 = \frac{\mu \lambda_{\min}^2}{L_f(1+L_p)\sqrt{\alpha_t \sigma_t^4}}$, After one gradient step $\hat{\mathbf{x}}_t = \mathbf{x}_t - \eta \nabla_{\mathbf{x}_t} \ell_t(\mathbf{x}_t)$, $\eta = \frac{\sqrt{\alpha_t}}{L_f(1+L_p)}$, we have $\ell_t(\hat{\mathbf{x}}_t) \leq (1 - \kappa_1)\ell_t(\mathbf{x}_t)$;*
3. *Consider a diffusion process that adheres to a bounded change in the objective function such that for any diffusion step, i.e., $\ell_{t-1}(\mathbf{x}_{t-1}) \leq \frac{\ell_t(\hat{\mathbf{x}}_t)}{(1-\kappa_2)}$ for some $\kappa_2 < \kappa_1$, then the objective function converges at a linear rate, i.e., $\ell_{t-1}(\mathbf{x}_{t-1}) \leq \frac{1-\kappa_1}{1-\kappa_2} \ell_t(\mathbf{x}_t)$.*

The proof is given in Appendix 8.2. The Lipschitz continuity and PL conditions are basic assumptions in optimization, and it has been shown that neural networks can locally satisfy these conditions [5]. Our next focus is on scenarios where the assumption in the third condition is met. Specifically, for large values

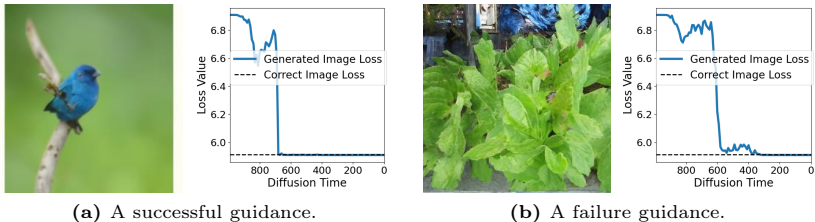


Fig. 1: The classifier loss of a successful and a failure guidance example. The target class is “indigo bird”.

of diffusion time t , the diffusion trajectory can exhibit substantial deviations between adjacent steps, leading to an increased value of κ_2 in the third condition. This phenomenon is less pronounced for smaller t . Consequently, the theorem leads us to anticipate a two-phase convergence pattern in training-free guidance: an initial phase where the loss remains relatively high and oscillates for larger t , followed by a swift decline (linear convergence) towards lower loss values as t decreases. In Figure 1, we use ResNet-50 trained on clean images to guide ImageNet pre-trained diffusion models. The loss value at each diffusion step is plotted. As a reference, we choose 100 images from the class “indigo bird” in ImageNet training set and compute the loss value, which is referred as “Correct Image Loss” in the figure. The two-stage convergence is verified by experiments. Remarkably, from theory and experiments, we see that training-free guidance can achieve low loss levels even in instances of guidance failure (Figure 1b). This is attributed to the influence of adversarial gradients, as discussed in the next subsection.

3.2 Limitations of Training-free Guidance

In this subsection, we examine the disadvantages of employing training-free guidance networks as opposed to training-based classifier guidance.

Training-free guidance is more sensitive to the adversarial gradient. Adversarial gradient is a significant challenge for neural networks, which refers to minimal perturbations deliberately applied to inputs that can induce disproportionate alterations in the model’s output [34]. The resilience of a model to adversarial gradients is often analyzed through the lens of its Lipschitz constant [31]. If the model has a lower Lipschitz constant, then it is less sensitive to the input perturbations and thus is more robust. In classifier guidance, time-dependent classifiers are trained on noise-augmented images. Our finding is that adding Gaussian noise transforms non-Lipschitz classifiers into Lipschitz ones. This transition mitigates the adversarial gradient challenge by inherently enhancing the model’s robustness to such perturbations, as shown in the next proposition.

Proposition 2. (*Time-dependent network is more robust and smooth*) Given a bounded non-Lipschitz loss function $\ell(\mathbf{x}) \leq C$, the loss $\hat{\ell}(\mathbf{x}) = \mathbb{E}_{\epsilon \sim \mathcal{N}(0, \mathbf{I})}[\ell(\mathbf{x} + \sigma_t \epsilon)]$ is $C \sqrt{\frac{2}{\pi \sigma_t^2}}$ -Lipschitz and $\nabla \hat{\ell}$ is $\frac{2C}{\sigma_t}$ -Lipschitz.

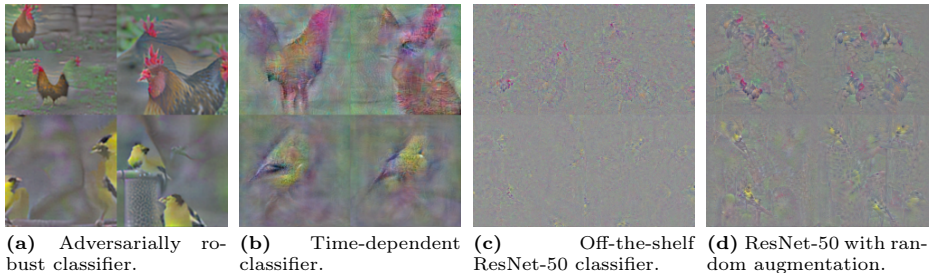


Fig. 2: Gradients of different classifiers on random backgrounds. The images in the first row correspond to the target class “cock”, and the second row to “goldfinch”.

The proof is given in Appendix 8.3. We present visualizations of the accumulated gradients for both the time-dependent and off-the-shelf time-independent classifiers corresponding to different classes in Figure 2b and Figure 2c, respectively. These visualizations are generated by initializing an image with a random background and computing 1000 gradient steps for each classifier. For the time-dependent classifier, the input time for the t -th gradient step is $1000 - t$. The images are generated purely by the classifier gradients without diffusion involved. For comparative analysis, we include the accumulated gradient of an adversarially robust classifier [30], as shown in Figure 2a, which has been specifically trained to resist adversarial gradients. The resulting plots reveal a stark contrast: the gradient of the time-dependent classifier visually resembles the target image, whereas the gradient of the time-independent classifier does not exhibit such recognizability. This observation suggests that off-the-shelf time-independent classifiers are prone to generating adversarial gradients compared to the time-dependent classifier used in classifier guidance. It could potentially misdirect the guidance process. In contrast to yielding a direction that meaningfully minimizes the loss, the adversarial gradient primarily serves to minimize the loss in a manner that is not necessarily aligned with the intended guidance direction.

Training-free guidance slows down the convergence of reverse ODE.

The efficiency of an algorithm in solving reverse ordinary differential equations is often gauged by the number of non-linear function estimations (NFEs) required to achieve convergence. This metric is vital for algorithmic design, as it directly relates to computational cost and time efficiency [32]. In light of this, we explore the convergence rates associated with various guidance paradigms, beginning our analysis with a reverse ODE framework that incorporates a generic gradient guidance term. The formula is expressed as

$$\frac{d\mathbf{x}_t}{dt} = f(t)\mathbf{x}_t + \frac{g^2(t)}{2}(\epsilon_\theta(\mathbf{x}_t, t) + \nabla_{\mathbf{x}_t} h(\mathbf{x}_t, t)), \quad (8)$$

where $h(\cdot, \cdot)$ can be either a time-dependent classifier or a time-independent classifier with Tweedie’s formula. The subsequent proposition elucidates the relationship between the discretization error and the smoothness of the guidance function.

Proposition 3. *Let $g(\mathbf{x}_t, t) = \epsilon_\theta(\mathbf{x}_t, t) + \nabla_{\mathbf{x}_t} h(\mathbf{x}_t, t)$ in (8). Assume that $g(\mathbf{x}_t, t)$ is L -Lipschitz. Then the discretization error of the DDIM solver is bounded by $O(h_{\max} + Lh_{\max})$, where $h_{\max} = \max_t \frac{1}{2} \left[\log\left(\frac{\alpha_t}{1-\alpha_t}\right) - \log\left(\frac{\alpha_{t-1}}{1-\alpha_{t-1}}\right) \right]$.*

The proof is given in Appendix 8.4. Proposition 2 establishes that time-dependent classifiers exhibit superior gradient Lipschitz constants compared to their off-the-shelf time-independent counterparts. This disparity in smoothness attributes leads to a deceleration in convergence for training-free guidance methods, necessitating a greater number of NFEs to achieve the desired level of accuracy when compared to classifier guidance.

4 Improving Training-free Guidance

This section presents enhancement techniques for improving training-free guidance, with theoretical justifications and empirical evidence.

Algorithm 1 Random Augmentation

```

for  $t = T, \dots, 0$  do
     $\mathbf{x}_{t-1} = \text{DDIM}(\mathbf{x}_t)$ 
     $\hat{\mathbf{x}}_0 = \frac{\mathbf{x}_t - \sigma_t \epsilon_\theta(\mathbf{x}_t, t)}{\sqrt{\alpha_t}}$ 
     $\mathbf{g}_t = \frac{1}{|\mathcal{T}|} \sum_{T \in \mathcal{T}} \nabla_{\mathbf{x}_t} \ell(f_\phi(T(\hat{\mathbf{x}}_0), \mathbf{y}))$ 
     $\mathbf{x}_{t-1} = \mathbf{x}_{t-1} - \eta \mathbf{g}_t$ 
end for

```

Algorithm 2 PGD

```

for  $t = T, \dots, 0$  do
     $\mathbf{x}_{t-1} = \text{DDIM}(\mathbf{x}_t)$ 
     $\hat{\mathbf{x}}_0 = \frac{\mathbf{x}_t - \sigma_t \epsilon_\theta(\mathbf{x}_t, t)}{\sqrt{\alpha_t}}$ 
     $\mathbf{g}_t = \nabla_{\mathbf{x}_t} \ell(f_\phi(\hat{\mathbf{x}}_0), \mathbf{y})$ 
     $\mathbf{x}_{t-1} = \mathbf{x}_{t-1} - \eta \cdot \frac{\mathbf{g}_t}{\|\mathbf{g}_t\|_2}$ 
end for

```

4.1 Randomized Augmentation

As established by Proposition 2, the introduction of Gaussian perturbations enhances the Lipschitz property of a neural network. A direct application of this principle involves creating multiple noisy instances of an estimated clean image and incorporating them into the guidance network, a method analogous to the one described in (6). However, given the high-dimensional nature of image data, achieving a satisfactory approximation of the expected value necessitates an impractically large number of noisy copies. To circumvent this issue, we propose an alternative strategy that employs a diverse set of data augmentations in place of solely adding Gaussian noise. This approach effectively introduces perturbations within a lower-dimensional latent space, thus requiring fewer samples. The suite of data augmentations utilized, denoted by \mathcal{T} , is derived from the differentiable data augmentation techniques outlined in [46], which encompasses transformations such as translation, resizing, color adjustments, and cutout operations. The details are shown in Algorithm 1 and the rationale is shown in the following proposition.

Proposition 4. (*Random augmentation improves smoothness*) Given a bounded non-Lipschitz loss function $\ell(\mathbf{x})$, the loss $\hat{\ell}(\mathbf{x}) = \mathbb{E}_{\epsilon \sim p(\epsilon)}[\ell(\mathbf{x} + \epsilon)]$ is $C \int_{\mathbb{R}^n} \|\nabla p(\mathbf{t})\|_2 d\mathbf{t}$ -Lipschitz and its gradient is $C \int_{\mathbb{R}^n} \|\nabla^2 p(\mathbf{t})\|_{op} d\mathbf{t}$ -Lipschitz.

The proof is shown in Appendix 8.5. Echoing the experimental methodology delineated in Section 3.2, we present an analysis of the accumulated gradient effects when applying random augmentation to a ResNet-50 model. Specifically, we utilize a set of $|\mathcal{T}| = 10$ diverse transformations as our augmentation strategy. The results of this experiment are visualized in Figure 2d, where the target object’s color and shape emerges in the gradient profile. This observation suggests that the implementation of random augmentation can alleviate the adversarial gradient issue.

4.2 Adaptive Gradient Scheduling

In Section 3.1, we established that the training guidance process can be conceptualized as the optimization of the loss function corresponding to the guidance network. Given this interpretation, it stands to reason that adopting a more sophisticated optimizer could accelerate the convergence of the guidance. Notably, the fundamental operation in guidance involves calculating the gradient of the guidance network with respect to the input, a procedure reminiscent of white-box adversarial attacks. Drawing inspiration from this parallel, we adopt the well-known Projected Gradient Descent (PGD) optimization technique—commonly employed in crafting adversarial examples—as our optimizer of choice, which is shown in Algorithm 2. We implement PGD within the context of a training-free guidance framework called FreeDoM [44] and benchmark the performance of this implementation using the DDIM sampler with 50 steps, ensuring identical seed initialization across the different methods for consistency.

As shown in Figure 3, FreeDoM is unable to effectively guide the generation process when faced with a significant discrepancy between the unconditional generation and the specified condition. An illustrative example is the difficulty in guiding the model to generate faces oriented to the left when the unconditionally generated faces predominantly orient to the right, as shown in the middle column of the figure. Conversely, when the unconditionally generated faces orient forward, the condition for any face orientation is more easily fulfilled. This challenge, which arises due to the insufficiency of 50 steps for convergence under the condition, is ameliorated by substituting gradient descent with PGD, thereby illustrating the benefits of employing an advanced optimizer in the guidance process.

4.3 Resampling Trick

The technique of resampling, also referred to as “time travel”, has been proposed as a solution to complex generative problems [24], facilitating successful training-free guidance in tasks such as CLIP-guided ImageNet generation and layout guidance for stable diffusion, as illustrated in Figure 2 of [44] and Figure 8 of [2],



Fig. 3: FreeDoM [44] with and without PGD trick. DDIM-50 is used for sampling.

respectively. The procedure of the resampling trick is shown in Algorithm 3, which involves recursive execution of individual sampling steps.

Algorithm 3 Resampling

```

1: for  $t = T, \dots, 1$  do
2:   for  $i = 1, \dots, s$  do
3:      $\mathbf{x}_{t-1}^i =$ 
       DDIM with Guidance( $\mathbf{x}_t^{i-1}$ )
4:     if  $i < s$  then
5:        $\beta_t = \alpha_t / \alpha_{t-1}, \mathbf{n} \sim \mathcal{N}(0, \mathbf{I})$ 
6:        $\mathbf{x}_t^i = \sqrt{\beta_t} \mathbf{x}_{t-1}^i + \sqrt{1 - \beta_t} \mathbf{n}$ 
7:     end if
8:      $\mathbf{x}_{t-1}^0 = \mathbf{x}_{t-1}^s$ 
9:   end for
10: end for

```

In this subsection, we endeavor to analyze the role of resampling in training-free guidance and thus complete the overall picture. During the diffusion process, samples can diverge from their target distributions due to various types of sampling error, such as adversarial gradient and discretization error. A critical component of the resampling process entails the reintroduction of random noise to transition the sample \mathbf{x}_{t-1} back to \mathbf{x}_t , effectively resetting the sampling state. The forthcoming lemma substantiates the premise that the act of adding identical noise to two vectors serves to diminish the disparity between the samples.

Lemma 1. (Adding noise removes the discrepancy; Lemma 7 of [42]) Suppose $\mathbf{n}_x, \mathbf{n}_y \sim \mathcal{N}(0, \sigma^2 \mathbf{I})$, and $\mathbf{x}' = \mathbf{x} + \mathbf{n}_x, \mathbf{y}' = \mathbf{y} + \mathbf{n}_y$. Then we have $TV(\mathbf{x}', \mathbf{y}') = 1 - 2Q(r)$, where $Q(\cdot)$ is Gaussian tail probability defined in Definition 3 in appendix and $r = \|\mathbf{x} - \mathbf{y}\| / (2\sigma)$.

Following Lemma 1, the next proposition demonstrates that the total variation distance between the sampled distribution $q_t(\mathbf{x}_t^i)$, as obtained in the i -th resampling of Algorithm 3, and the ground-truth distribution $p_t(\mathbf{x}_t)$, is progressively reduced through recursive application of the resampling steps.

Proposition 5. Denote $p_t(\mathbf{x}_t)$ and $q_t(\mathbf{x}_t)$ as the ground-truth distribution and the distribution distribution sampled by Algorithm 3, and $2\|\mathbf{x}_t\| \leq B$. Then we have

$$TV(q_t(\mathbf{x}_t^s), p_t(\mathbf{x}_t)) \leq \left(1 - 2Q\left(\frac{\sqrt{\beta_t} B}{2\sqrt{1 - \beta_t}}\right)\right)^{s-1} TV(q_t(\mathbf{x}_t^1), p_t(\mathbf{x}_t)) + O(h_{\max}),$$

where h_{\max} is defined in Proposition 3.

The proof is presented in Appendix 8.6. Proposition 5 indicates that the resampling technique serves to “rectify” the distributional divergence caused by guidance. This aspect is crucial, as we have demonstrated that training-free guidance is particularly susceptible to adversarial gradients, which steer the images away from the natural image distribution. The resampling technique realigns these images with the distribution of natural images. This theoretical insight is corroborated by the empirical evidence presented in Figure 2 of [44].

5 Experiments

In this section, we evaluate the efficacy of our proposed techniques across various diffusion models, including CeleA-HQ, ImageNet, and text-to-motion, under different conditions such as sketch, segmentation, text, and object avoidance. We compare our methods with established baselines: Universal Guidance (UG) [2], Loss-Guided Diffusion with Monte Carlo (LGD-MC) [33], and Training-Free Energy-Guided Diffusion Models (FreeDoM) [44]. UG employs guidance as delineated in (5) and uses resampling strategies outlined in Algorithm 3 to enhance performance. Similarly, FreeDoM is founded on (5) and resampling. In addition, FreeDoM incorporates a time-dependent step size for each gradient guidance and judiciously selects the diffusion step for executing resampling. LGD-MC also utilizes guidance from (6), setting the $n = 10$. For the sampling process, we employ the DDIM method with 100 steps, consistent with the protocols in FreeDoM and LGD-MC papers. We have developed our approach based on FreeDoM, with the inclusion of random augmentation (Algorithm 1) and projected gradient descent (Algorithm 2).

5.1 Guidance to CelebA-HQ Diffusion

In this subsection, we adopt the experimental setup from [44]. Specifically, we utilize the CelebA-HQ diffusion model [14] to generate high-quality facial images. We explore three guidance conditions: segmentation, sketch, and text. For segmentation guidance, BiSeNet [43] generates the facial segmentation maps, with an ℓ_2 -loss applied between the estimated map of the synthesized image and the provided map. Sketch guidance involves using the method from [41] to produce facial sketches, where the loss function is the ℓ_2 -loss between the estimated sketch of \hat{x}_0 and the given sketch. For text guidance, we employ CLIP [28] as both the image and text encoders, setting the loss to be the ℓ_2 distance between the image and text embeddings.

For benchmarking, we preprocess the CelebA-HQ dataset with BiSeNet to extract segmentation maps and use the model checkpoint from [41] to acquire the sketches. We randomly select 1000 samples each of segmentation maps, sketches, and text descriptions. The comparative results are presented in Table 1. Consistent with [44], the resampling number for both FreeDoM and UG is set to $s = 1$. Figure 4 displays a random selection of the generated images. More image samples are provided in the supplementary materials.

| Methods | Segmentation maps | | Sketches | | Texts | |
|--------------|-------------------|--------------|--------------|--------------|--------------|--------------|
| | Distance↓ | FID↓ | Distance↓ | FID↓ | Distance↓ | FID↓ |
| UG [2] | 2247.2 | 39.91 | 52.15 | 47.20 | 12.08 | 44.27 |
| LGD-MC [33] | 2088.5 | 38.99 | 49.46 | 54.47 | 11.84 | 41.74 |
| FreeDoM [44] | 1657.0 | 38.65 | 34.21 | 52.18 | 11.17 | 46.13 |
| Ours | 1575.7 | 33.31 | 30.41 | 41.26 | 10.72 | 41.25 |

Table 1: The performance comparison of various methods on CelebA-HQ with different types of zero-shot guidance. The experimental settings adhere to Table 1 of [44].

| Methods | LGD-MC [33] | UG [2] | FreeDoM [44] | Ours |
|-------------|-------------|--------|--------------|-------------|
| CLIP Score↑ | 24.3 | 25.7 | 25.9 | 27.7 |

Table 2: The performance comparison of various methods on unconditional ImageNet with zero-shot text guidance. We compare various methods using ImageNet pre-trained diffusion models with CLIP-B/16 guidance. For evaluating performance, the CLIP score is computed using CLIP-L/14.

5.2 Guidance to ImageNet Diffusion

For the unconditional ImageNet diffusion, we employ text guidance in line with the approach used in FreeDoM and UG [2, 44]. We utilize CLIP-B/16 as the image and text encoder, with cosine similarity serving as the loss function to measure the congruence between the image and text embeddings. To evaluate performance and mitigate the potential for high-scoring adversarial images, we use CLIP-L/14 for computing the CLIP score. In FreeDoM, resampling is conducted for time steps ranging from 800 to 300, with the number of resamplings fixed at 10, as described in [44]. Given that UG resamples at every step, we adjust its resampling number $s = 5$ to align the execution time with that of FreeDoM. The textual prompts for our experiments are sourced from [10, 21]. The comparison of different methods is depicted in Table 2. The corresponding randomly selected images are illustrated in Figure 5. The table indicates that our method achieves the highest consistency with the provided prompts. As shown in Figure 5, LGD-MC tends to overlook elements of the prompts. Both UG and FreeDoM occasionally produce poorly shaped animals, likely influenced by adversarial gradients. Our approach addresses this issue through the implementation of random augmentation. Additionally, none of the methods successfully generate images that accurately adhere to positional prompts such as “left to” or “below”. This limitation is inherent to CLIP and extends to all text-to-image generative models [37]. More image samples are provided in the supplementary materials.

5.3 Guidance to Human Motion Diffusion

In this subsection, we extend our evaluation to human motion generation using the Motion Diffusion Model (MDM) [36], which represents motion through a sequence of joint coordinates and is trained on a large corpus of text-motion pairs with classifier-free guidance. We apply the object avoidance guidance as

| Methods | “Backwards” | | “Balanced Beam” | | “Walking” | | “Jogging” | |
|--------------------|------------------|--------------|------------------|-------------|------------------|--------------|------------------|--------------|
| | Loss↓ | CLIP↑ | Loss↓ | CLIP↑ | Loss↓ | CLIP↑ | Loss↓ | CLIP↑ |
| Unconditional [36] | 3.55 + 9.66 | 65.6 | 47.92 + 0 | 70.8 | 48.88 + 0 | 37.6 | 144.84 + 0 | 61.72 |
| FreeDoM [44] | 1.09 + 6.63 | 67.23 | 9.83 + 4.48 | 62.65 | 1.64 + 7.55 | 40.12 | 34.95 + 7.83 | 58.74 |
| LGD-MC [33] | 0.98 + 6.48 | 67.31 | 4.42 + 0.02 | 63.13 | 1.30 + 0.39 | 38.82 | 6.12 + 2.38 | 57.89 |
| Ours | 0.68+1.32 | 67.50 | 1.13+0.30 | 63.02 | 0.43+0.31 | 40.40 | 2.93+1.15 | 60.03 |

Table 3: Comparison of various methods on MDM with zero-shot targeting and object avoidance guidance. Loss is reported as a two-component metric: the first part is the MSE between the target and the actual final position of the individual; the second part measures the object avoidance loss.

described in [33]. Let $\mathbf{x}_0(t)$ denote the joint coordinates at time t , \mathbf{y}_t the target location, \mathbf{y}_{obs} the obstacle location, r the radius of the objects, and T the total number of frames. The loss function is defined as follows:

$$\ell = \|\mathbf{y}_t - \mathbf{x}_0(T)\|_2^2 + \sum_i \text{sigmoid}(-(\|\mathbf{x}_0(i) - \mathbf{y}_{\text{obs}}\| - r) \times 50) \times 100. \quad (9)$$

Our experimental configuration adheres to the guidelines set forth in [33]. We assess the methods using the targeting loss (the first term in (9)), the object avoidance loss (the second term in (9)), and the CLIP score calculated by MotionCLIP [35]. For FreeDoM, the number of resamplings is set to 3. In our method, random augmentation is omitted because the guidance is not computed by neural networks so the adversarial gradient issues are absent. The quantitative results of our investigation are summarized in Table 3, while Figure 6 showcases randomly selected samples. Our methods exhibit enhanced control quality over the generated motion. The videos are provided in the supplementary materials.

6 Conclusions

In this paper, we conducted a comprehensive investigation into training-free guidance, which employs pre-trained diffusion models and guides them using the off-the-shelf trained on clean images. Our exploration delved into the underlying mechanisms and fundamental limits of these models. Moreover, we proposed a set of enhancement techniques and verified their effectiveness both theoretically and empirically.

Limitations. Despite our efforts to mitigate the shortcomings of training-free methods and enhance their performance, certain intractable limitations remain. Notably, the refined training-free guidance still necessitates a higher number of NFEs when compared with extensive training methods such as classifier-free guidance. This is because adversarial gradient cannot be fully eliminated without training.

Ethical Consideration. Similar to other models designed for image creation, our model also has the unfortunate potential to be used for creating deceitful or damaging material. We pledge to restrict the usage of our model exclusively to the realm of research to prevent such misuse.

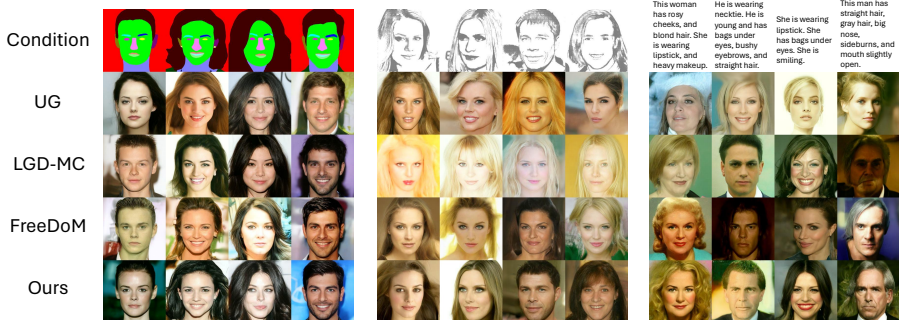


Fig. 4: Qualitative results of CelebA-HQ with zero-shot segmentation, sketch, and text guidance. The images are randomly selected.



Fig. 5: Qualitative results of ImageNet model with zero-shot text guidance. The images are randomly selected.

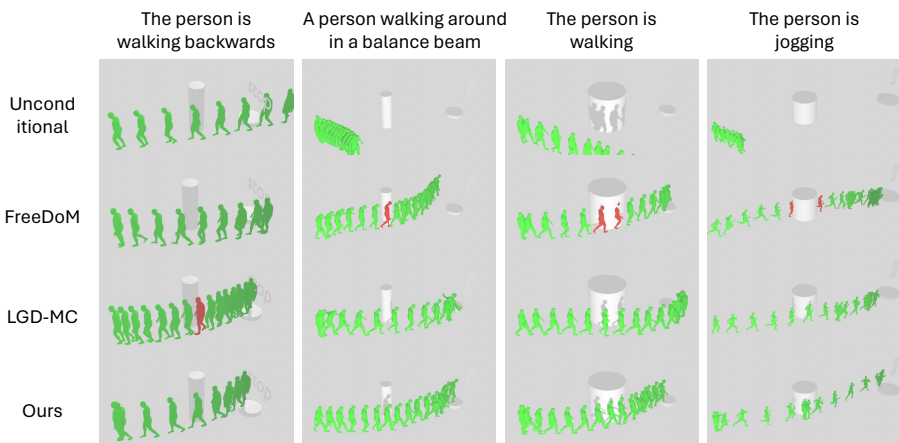


Fig. 6: Qualitative results of human motion diffusion with zero-shot object avoidance and targeting guidance. Instances of intersection with obstacles are highlighted by marking the person in red. The trajectories are randomly selected.

References

1. Athalye, A., Engstrom, L., Ilyas, A., Kwok, K.: Synthesizing robust adversarial examples. In: International conference on machine learning. pp. 284–293. PMLR (2018) **19**
2. Bansal, A., Chu, H.M., Schwarzschild, A., Sengupta, S., Goldblum, M., Geiping, J., Goldstein, T.: Universal guidance for diffusion models. In: Proceedings of the IEEE/CVF Conference on Computer Vision and Pattern Recognition. pp. 843–852 (2023) **2, 4, 9, 11, 12, 18**
3. Brooks, T., Peebles, B., Homes, C., DePue, W., Guo, Y., Jing, L., Schnurr, D., Taylor, J., Luhman, T., Luhman, E., Ng, C., Wang, R., Ramesh, A.: Video generation models as world simulators (2024), <https://openai.com/research/video-generation-models-as-world-simulators> **1**
4. Chakraborty, A., Alam, M., Dey, V., Chattopadhyay, A., Mukhopadhyay, D.: Adversarial attacks and defences: A survey. arXiv preprint arXiv:1810.00069 (2018) **19**
5. Chen, Y., Shi, Y., Dong, M., Yang, X., Li, D., Wang, Y., Dick, R., Lv, Q., Zhao, Y., Yang, F., et al.: Over-parameterized model optimization with polyak-łojasiewicz condition (2023) **5**
6. Chung, H., Kim, J., McCann, M.T., Klasky, M.L., Ye, J.C.: Diffusion posterior sampling for general noisy inverse problems. arXiv preprint arXiv:2209.14687 (2022) **4**
7. Dhariwal, P., Nichol, A.: Diffusion models beat gans on image synthesis. Advances in neural information processing systems **34**, 8780–8794 (2021) **1, 2, 4**
8. Dong, Y., Liao, F., Pang, T., Su, H., Zhu, J., Hu, X., Li, J.: Boosting adversarial attacks with momentum. In: Proceedings of the IEEE conference on computer vision and pattern recognition. pp. 9185–9193 (2018) **19**
9. Epstein, D., Jabri, A., Poole, B., Efros, A., Holynski, A.: Diffusion self-guidance for controllable image generation. Advances in Neural Information Processing Systems **36** (2024) **18**
10. Feng, W., He, X., Fu, T.J., Jampani, V., Akula, A., Narayana, P., Basu, S., Wang, X.E., Wang, W.Y.: Training-free structured diffusion guidance for compositional text-to-image synthesis. arXiv preprint arXiv:2212.05032 (2022) **12**
11. Goodfellow, I.J., Shlens, J., Szegedy, C.: Explaining and harnessing adversarial examples. arXiv preprint arXiv:1412.6572 (2014) **19**
12. Han, X., Shan, C., Shen, Y., Xu, C., Yang, H., Li, X., Li, D.: Training-free multi-objective diffusion model for 3d molecule generation. In: The Twelfth International Conference on Learning Representations (2023) **18**
13. Hertz, A., Mokady, R., Tenenbaum, J., Aberman, K., Pritch, Y., Cohen-Or, D.: Prompt-to-prompt image editing with cross attention control. arXiv preprint arXiv:2208.01626 (2022) **18**
14. Ho, J., Jain, A., Abbeel, P.: Denoising diffusion probabilistic models. Advances in neural information processing systems **33**, 6840–6851 (2020) **11**
15. Ho, J., Salimans, T.: Classifier-free diffusion guidance. arXiv preprint arXiv:2207.12598 (2022) **2**
16. Hoogeboom, E., Satorras, V.G., Vignac, C., Welling, M.: Equivariant diffusion for molecule generation in 3d. In: International conference on machine learning. pp. 8867–8887. PMLR (2022) **1**
17. Janner, M., Du, Y., Tenenbaum, J., Levine, S.: Planning with diffusion for flexible behavior synthesis. In: International Conference on Machine Learning. pp. 9902–9915. PMLR (2022) **1, 19**

18. Karimi, H., Nutini, J., Schmidt, M.: Linear convergence of gradient and proximal-gradient methods under the polyak-lojasiewicz condition. In: Machine Learning and Knowledge Discovery in Databases: European Conference, ECML PKDD 2016, Riva del Garda, Italy, September 19-23, 2016, Proceedings, Part I 16. pp. 795–811. Springer (2016) [20](#)
19. Liang, Z., Mu, Y., Ding, M., Ni, F., Tomizuka, M., Luo, P.: Adaptdiffuser: Diffusion models as adaptive self-evolving planners. arXiv preprint arXiv:2302.01877 (2023) [1](#)
20. Liu, X., Park, D.H., Azadi, S., Zhang, G., Chopikyan, A., Hu, Y., Shi, H., Rohrbach, A., Darrell, T.: More control for free! image synthesis with semantic diffusion guidance. In: Proceedings of the IEEE/CVF Winter Conference on Applications of Computer Vision. pp. 289–299 (2023) [4](#), [19](#)
21. Liu, X., Gong, C., Wu, L., Zhang, S., Su, H., Liu, Q.: Fusedream: Training-free text-to-image generation with improved clip+ gan space optimization. arXiv preprint arXiv:2112.01573 (2021) [12](#)
22. Lu, C., Chen, H., Chen, J., Su, H., Li, C., Zhu, J.: Contrastive energy prediction for exact energy-guided diffusion sampling in offline reinforcement learning. arXiv preprint arXiv:2304.12824 (2023) [4](#), [19](#)
23. Lu, C., Zhou, Y., Bao, F., Chen, J., Li, C., Zhu, J.: Dpm-solver: A fast ode solver for diffusion probabilistic model sampling in around 10 steps. Advances in Neural Information Processing Systems **35**, 5775–5787 (2022) [21](#)
24. Lugmayr, A., Danelljan, M., Romero, A., Yu, F., Timofte, R., Van Gool, L.: Repaint: Inpainting using denoising diffusion probabilistic models. In: Proceedings of the IEEE/CVF Conference on Computer Vision and Pattern Recognition. pp. 11461–11471 (2022) [9](#)
25. Madry, A., Makelov, A., Schmidt, L., Tsipras, D., Vladu, A.: Towards deep learning models resistant to adversarial attacks. arXiv preprint arXiv:1706.06083 (2017) [19](#)
26. Miyasawa, K., et al.: An empirical bayes estimator of the mean of a normal population. Bull. Inst. Internat. Statist **38**(181-188), 1–2 (1961) [5](#)
27. Mo, S., Mu, F., Lin, K.H., Liu, Y., Guan, B., Li, Y., Zhou, B.: Freecontrol: Training-free spatial control of any text-to-image diffusion model with any condition. arXiv preprint arXiv:2312.07536 (2023) [18](#)
28. Radford, A., Kim, J.W., Hallacy, C., Ramesh, A., Goh, G., Agarwal, S., Sastry, G., Askell, A., Mishkin, P., Clark, J., et al.: Learning transferable visual models from natural language supervision. In: International conference on machine learning. pp. 8748–8763. PMLR (2021) [11](#)
29. Rombach, R., Blattmann, A., Lorenz, D., Esser, P., Ommer, B.: High-resolution image synthesis with latent diffusion models. In: Proceedings of the IEEE/CVF conference on computer vision and pattern recognition. pp. 10684–10695 (2022) [1](#)
30. Salman, H., Ilyas, A., Engstrom, L., Kapoor, A., Madry, A.: Do adversarially robust imagenet models transfer better? Advances in Neural Information Processing Systems **33**, 3533–3545 (2020) [7](#)
31. Salman, H., Li, J., Razenshteyn, I., Zhang, P., Zhang, H., Bubeck, S., Yang, G.: Provably robust deep learning via adversarially trained smoothed classifiers. Advances in Neural Information Processing Systems **32** (2019) [6](#), [21](#)
32. Song, J., Meng, C., Ermon, S.: Denoising diffusion implicit models. arXiv preprint arXiv:2010.02502 (2020) [7](#)
33. Song, J., Zhang, Q., Yin, H., Mardani, M., Liu, M.Y., Kautz, J., Chen, Y., Vahdat, A.: Loss-guided diffusion models for plug-and-play controllable generation (2023) [2](#), [4](#), [5](#), [11](#), [12](#), [13](#), [18](#)

34. Szegedy, C., Zaremba, W., Sutskever, I., Bruna, J., Erhan, D., Goodfellow, I., Fergus, R.: Intriguing properties of neural networks. arXiv preprint arXiv:1312.6199 (2013) [6](#)
35. Tevet, G., Gordon, B., Hertz, A., Bermano, A.H., Cohen-Or, D.: Motionclip: Exposing human motion generation to clip space. In: European Conference on Computer Vision. pp. 358–374. Springer (2022) [13](#)
36. Tevet, G., Raab, S., Gordon, B., Shafir, Y., Cohen-Or, D., Bermano, A.H.: Human motion diffusion model. arXiv preprint arXiv:2209.14916 (2022) [12](#), [13](#)
37. Tong, S., Jones, E., Steinhardt, J.: Mass-producing failures of multimodal systems with language models. Advances in Neural Information Processing Systems **36** (2024) [12](#)
38. Tumanyan, N., Geyer, M., Bagon, S., Dekel, T.: Plug-and-play diffusion features for text-driven image-to-image translation. In: Proceedings of the IEEE/CVF Conference on Computer Vision and Pattern Recognition. pp. 1921–1930 (2023) [18](#)
39. Vershynin, R.: High-dimensional probability: An introduction with applications in data science, vol. 47. Cambridge university press (2018) [5](#)
40. Wang, W., Han, D., Luo, X., Shen, Y., Ling, C., Wang, B., Li, D.: Toward open-ended embodied tasks solving. In: NeurIPS 2023 Agent Learning in Open-Endedness Workshop (2023) [2](#), [18](#)
41. Xiang, X., Liu, D., Yang, X., Zhu, Y., Shen, X., Allebach, J.P.: Adversarial open domain adaptation for sketch-to-photo synthesis. In: Proceedings of the IEEE/CVF Winter Conference on Applications of Computer Vision (2022) [11](#)
42. Xu, Y., Deng, M., Cheng, X., Tian, Y., Liu, Z., Jaakkola, T.: Restart sampling for improving generative processes. Advances in Neural Information Processing Systems **36** (2024) [10](#), [22](#)
43. Yu, C., Wang, J., Peng, C., Gao, C., Yu, G., Sang, N.: Bisenet: Bilateral segmentation network for real-time semantic segmentation. In: Proceedings of the European conference on computer vision (ECCV). pp. 325–341 (2018) [11](#)
44. Yu, J., Wang, Y., Zhao, C., Ghanem, B., Zhang, J.: Freedom: Training-free energy-guided conditional diffusion model. arXiv preprint arXiv:2303.09833 (2023) [2](#), [4](#), [9](#), [10](#), [11](#), [12](#), [13](#), [18](#)
45. Zhang, L., Rao, A., Agrawala, M.: Adding conditional control to text-to-image diffusion models. In: Proceedings of the IEEE/CVF International Conference on Computer Vision. pp. 3836–3847 (2023) [1](#)
46. Zhao, S., Liu, Z., Lin, J., Zhu, J.Y., Han, S.: Differentiable augmentation for data-efficient gan training. Advances in neural information processing systems **33**, 7559–7570 (2020) [8](#)
47. Zheng, S., He, J., Liu, C., Shi, Y., Lu, Z., Feng, W., Ju, F., Wang, J., Zhu, J., Min, Y., et al.: Towards predicting equilibrium distributions for molecular systems with deep learning. arXiv preprint arXiv:2306.05445 (2023) [1](#)

7 Related Works and Discussions

7.1 Training-Free Control for Diffusion

The current training-free control strategies for diffusion models can be divided into two primary categories. The first category is the investigated topic in this paper, which is universally applicable to universal control formats and diffusion models. These methods predict a clean image, subsequently leveraging pre-trained networks to guide the diffusion process. Central to this approach are the algorithms based on (5), which have been augmented through techniques like resampling [2, 44] and the introduction of Gaussian noise [33]. Extensions of these algorithms have found utility in domains with constrained data-condition pairs, such as molecule generation [12], and in scenarios necessitating zero-shot guidance, like open-ended goals in offline reinforcement learning [40]. In molecular generation and offline reinforcement learning, they outperform training-based alternatives as additional training presents challenges. This paper delves deeper into the mechanics of this paradigm and introduces a suite of enhancements to bolster its performance. The efficacy of our proposed modifications is demonstrated across image and motion generation, with promising potential for generalization to molecular modeling and reinforcement learning tasks.

The second category of training-free control is tailored to text-to-image or text-to-video diffusion models, which is based on insights into their internal backbone architecture. For instance, object layout and shape have been linked to the cross-attention mechanisms [13], while network activations have been shown to preserve object appearance [38]. These understandings facilitate targeted editing of object layout and appearance (Diffusion Self-Guidance [9]) and enable the imposition of conditions in ControlNet through training-free means (FreeControl [27]). Analyzing these methodologies is challenging due to their reliance on emergent representations during training. Nonetheless, certain principles from this paper remain relevant; for example, as noted in Proposition 3, these methods often necessitate extensive diffusion steps, with instances such as [9, 27] employing 1000 steps. A thorough examination and refinement of these techniques remain an avenue for future research.

7.2 Training-based Gradient Guidance

The training-based gradient guidance paradigm, such as classifier guidance, is a predominant approach for diffusion guidance. The core objective is to train a time-dependent network that approximates $p_t(\mathbf{y}|\mathbf{x}_t)$ in the RHS of (2), and to utilize the resulting gradient as guidance. The most well-known example is classifier guidance, which involves training a classifier on noisy images. However, classifier guidance is limited to class conditions and is not adaptable to other forms of control, such as image and text guidance. To address this limitation, there are two main paradigms. The first involves training a time-dependent

network that aligns features extracted from both clean and noisy images, as described by [20]. The training process is outlined as follows:

$$\min_{\psi} \mathbb{E}_{p(\mathbf{x}_0, \mathbf{x}_t)} d(f_{\psi}(\mathbf{x}_t, t), f_{\phi}(\mathbf{x}_0)),$$

where $d(\cdot, \cdot)$ represents a loss function, such as cross-entropy or the ℓ_2 norm. If time-dependent networks for clean images are already available, training can proceed in a self-supervised fashion without the need for labeled data. The second paradigm, as outlined by [17], involves training an energy-based model to approximate $p_t(\mathbf{y}|\mathbf{x}_t)$. The training process is described as follows:

$$\min_{\psi} \mathbb{E}_{p(\mathbf{x}_0, \mathbf{x}_t)} |\ell(f_{\psi}(\mathbf{x}_t, t), \mathbf{y}) - \ell(f_{\phi}(\mathbf{x}_0), \mathbf{y})|.$$

However, it is observed in [22] that none of these methods can accurately approximate the true energy in (4). The authors of [22] propose an algorithm to learn the true energy. The loss function is a contrastive loss

$$\min_{\psi} \mathbb{E}_{p(\mathbf{x}_0^i, \mathbf{x}_t^i)} \exp(-\ell(f_{\phi}(\mathbf{x}_0), \mathbf{y})) \left[-\sum_{i=1}^K \log \frac{\exp(\ell(f_{\psi}(\mathbf{x}_t^i, t), \mathbf{y}^i))}{\sum_{j=1}^K \exp(-\ell(f_{\psi}(\mathbf{x}_t^j, t), \mathbf{y}^j))} \right],$$

where $(\mathbf{x}_0^i, \mathbf{x}_t^i)$ are K paired data samples from $p(\mathbf{x}_0^i, \mathbf{y}^i)$. Theorem 3.2 in [22] proves that the optimal f_{ψ^*} satisfied that $\nabla_{\mathbf{x}_t} \ell(f_{\psi^*}(\mathbf{x}_t^i, t), \mathbf{y}^i) = \nabla_{\mathbf{x}_t} p_t(\mathbf{y}|\mathbf{x}_t)$.

Although this paper focuses on training-free guidance, the findings in this paper can be naturally extended to all training-based gradient guidance schemes. Firstly, the issue of adversarial gradients cannot be resolved without additional training; hence, all the aforementioned methods are subject to adversarial gradients. Empirical evidence for this is presented in Fig. 2, which illustrates that the gradients from an adversarially robust classifier are markedly more vivid than those from time-dependent classifiers. Consequently, it is anticipated that incorporating additional adversarial training into these methods would enhance the quality of the generated samples. Secondly, since these methods are dependent on gradients, employing a more sophisticated gradient solver could further improve their NFEs.

7.3 Adversarial Attack and Robustness

Adversarial attacks and robustness constitute a fundamental topic in deep learning [4]. An adversarial attack introduces minimal, yet strategically calculated, changes to the original data that are often imperceptible to humans, leading models to make incorrect predictions. The most common attacks are gradient-based, for example, the Fast Gradient Sign Method (FGSM) [11], Projected Gradient Descent (PGD) [25], Smoothed Gradient Attacks [1], and Momentum-Based Attacks [8]. An attack is akin to classifier guidance or training-free guidance, which uses the gradient of a pre-trained network for guidance. Should the gradient be adversarial, the guidance will be compromised. This paper establishes the

relationship between training-free loss-guided diffusion models and adversarial attacks in two ways. Firstly, we prove that training-free guidance is more sensitive to an adversarial gradient. Secondly, in Section 4.2, we demonstrate that borrowing a superior solver from the adversarial attack literature expedites the convergence of the diffusion ODE.

8 Proofs

8.1 Definitions

This subsection introduces a few definitions that are useful in the following sections.

Definition 1. (*L-Lipschitz*) A function $f : \mathbb{R}^n \rightarrow \mathbb{R}^m$ is said to be *L-Lipschitz* if there exists a constant $L \geq 0$ such that $\|f(\mathbf{x}_2) - f(\mathbf{x}_1)\| \leq L\|\mathbf{x}_2 - \mathbf{x}_1\|$ for all $\mathbf{x}_1, \mathbf{x}_2 \in \mathbb{R}^n$.

Definition 2. (*PL condition*) A function $f : \mathbb{R}^n \rightarrow \mathbb{R}$ satisfies *PL condition* with parameter μ if $\|\nabla f(\mathbf{x})\|^2 \geq \mu f(\mathbf{x})$.

Definition 3. (*Q function*) We define the *Gaussian tail probability* $Q(x) = \mathbb{P}(x \geq a)$, $x \sim \mathcal{N}(0, 1)$.

8.2 Proof for Proposition 1

For the first condition, the Lipschitz constant satisfies

$$\begin{aligned} |\ell_t(\mathbf{x}_1) - \ell_t(\mathbf{x}_2)| &\leq \frac{L_f}{\sqrt{\alpha_t}} |\mathbf{x}_1 - \nabla_{\mathbf{x}_1} \log p_t(\mathbf{x}_1) - \mathbf{x}_2 + \nabla_{\mathbf{x}_2} \log p_t(\mathbf{x}_2)| \\ &\leq L_f(1 + L_p)\|\mathbf{x}_1 - \mathbf{x}_2\|, \end{aligned}$$

and the PL constant satisfies

$$\ell_t(\mathbf{x}_t) \leq \frac{1}{\mu} \left\| \frac{\partial \ell}{\partial \hat{\mathbf{x}}_0} \right\|^2 = \frac{1}{\mu} \|\nabla_{\mathbf{x}_t} \ell \cdot \text{Cov}^{-1}(\mathbf{x}_0|\mathbf{x}_t) \sigma_t^2 \sqrt{\alpha_t}\|^2 \leq \frac{\sigma_t^4 \alpha_t}{\mu \lambda_{\min}^2} \|\nabla_{\mathbf{x}_t} \ell\|^2.$$

The second and third conditions directly follow Lemma 2.

Lemma 2. (*Linear Convergence Under PL condition; [18]*) Denote \mathbf{x}^0 as the initial point and \mathbf{x}^t as the point after t gradient steps. If the function is *L-Lipschitz* and μ -*PL*, gradient descent with a step size $\eta = \frac{1}{L}$ converges to a global solution with $\ell(\mathbf{x}^t) \leq (1 - \mu/L)^t \ell(\mathbf{x}^0)$.

8.3 Proof for Proposition 2

Proof. The proof of this theorem is based on the proof of Lemma 1 in [31]. By the definition of expectation, we have

$$\begin{aligned}\hat{f}(\mathbf{x}) &= \mathbb{E}_{\boldsymbol{\epsilon} \sim \mathcal{N}(0, \mathbf{I})}[f(\mathbf{x} + \sigma_t \boldsymbol{\epsilon})] = (f \otimes \mathcal{N}(0, \sigma_t^2 \mathbf{I}))(\mathbf{x}) \\ &= \frac{1}{(2\pi\sigma_t^2)^{n/2}} \int_{\mathbb{R}^n} f(\mathbf{z}) \exp\left(-\frac{1}{2\sigma_t^2} \|\mathbf{x} - \mathbf{z}\|^2\right) d\mathbf{z}.\end{aligned}$$

We then show that for any unit direction \mathbf{u} , $\mathbf{u}^T \nabla \hat{f}(\mathbf{x}) \leq \sqrt{\frac{2}{\pi\sigma_t^2}}$. The derivative of \hat{f} is given by

$$\begin{aligned}\nabla \hat{f}(\mathbf{x}) &= \frac{1}{(2\pi\sigma_t^2)^{n/2}} \int_{\mathbb{R}^n} f(\mathbf{z}) \nabla \exp\left(-\frac{1}{2\sigma_t^2} \|\mathbf{x} - \mathbf{z}\|^2\right) d\mathbf{z} \\ &= \frac{1}{(2\pi\sigma_t^2)^{n/2} \sigma_t^2} \int_{\mathbb{R}^n} f(\mathbf{z}) (\mathbf{x} - \mathbf{z}) \exp\left(-\frac{1}{2\sigma_t^2} \|\mathbf{x} - \mathbf{z}\|^2\right) d\mathbf{z}.\end{aligned}$$

Thus, the Lipschitz constant is computed as

$$\begin{aligned}\mathbf{u}^T \nabla \hat{f}(\mathbf{x}) &\leq \frac{C}{(2\pi\sigma_t^2)^{n/2}} \int_{\mathbb{R}^n} |\mathbf{u}^T (\mathbf{x} - \mathbf{z}) / \sigma_t^2| \exp\left(-\frac{1}{2\sigma_t^2} \|\mathbf{x} - \mathbf{z}\|^2\right) d\mathbf{z} \\ &= \frac{C}{(2\pi\sigma_t^2)^{1/2}} \int_{-\infty}^{\infty} |s| \exp\left(-\frac{1}{2}s^2\right) ds = \sqrt{\frac{2}{\pi\sigma_t^2}}.\end{aligned}$$

Similarly, for the Lipschitz constant of the gradient, we have

$$\begin{aligned}\|\nabla^2 \hat{f}(\mathbf{x})\|_{\text{op}} &\leq \|\nabla^2 \hat{f}(\mathbf{x})\|_2 \\ &\leq \frac{C}{\sqrt{2\pi\sigma_t} \cdot \sigma_t^4} \left(\int_{-\infty}^{\infty} s^2 \exp\left(-\frac{1}{2}s^2/\sigma_t^2\right) ds + \int_{-\infty}^{\infty} \sigma_t^2 \exp\left(-\frac{1}{2}s^2/\sigma_t^2\right) ds \right) = \frac{2C}{\sigma_t}.\end{aligned}$$

8.4 Proof for Proposition 3

Proof. We first analyze the discretization error of a single step from time s to t . We denote the update variable for DDIM is \mathbf{x}_t^* and the optimal solution of the diffusion ODE at time t as \mathbf{x}_t^* . Let $\sigma_t = \sqrt{1 - \alpha_t}$, $\lambda_t = \frac{1}{2} \log\left(\frac{\alpha_t}{1 - \alpha_t}\right)$ and $h = \lambda_t - \lambda_s$. According to (B.4) of [23], the update of DDIM solver is given by

$$\mathbf{x}_t = \sqrt{\frac{\alpha_t}{\alpha_s}} \mathbf{x}_s - \sigma_t (e^h - 1) \boldsymbol{\epsilon}_\theta(\mathbf{x}_s, s).$$

A similar relationship can be obtained for the optimal solution

$$\mathbf{x}_t^* = \sqrt{\frac{\alpha_t}{\alpha_s}} \mathbf{x}_s^* - \sigma_t (e^h - 1) \boldsymbol{\epsilon}_\theta(\mathbf{x}_s^*, s) + O(h^2).$$

We then bound the error between \mathbf{x}_t and \mathbf{x}_t^* . We have

$$\begin{aligned} \mathbf{x}_t &\leq \sqrt{\frac{\alpha_t}{\alpha_s}} \mathbf{x}_s - \sigma_t(e^h - 1)(\epsilon_\theta(\mathbf{x}_s^*, s) + L(\mathbf{x}_s - \mathbf{x}_s^*)) \\ &= \sqrt{\frac{\alpha_t}{\alpha_s}} \mathbf{x}_s^* - \sigma_t(e^h - 1)\epsilon_\theta(\mathbf{x}_s^*, s) + \sqrt{\frac{\alpha_t}{\alpha_s}}(\mathbf{x}_t - \mathbf{x}_s^*) - \sigma_t(e^h - 1)L(\mathbf{x}_s - \mathbf{x}_s^*) \\ &= \mathbf{x}_t^* + O(h^2) + O(Lh^2). \end{aligned}$$

If we run DDIM for M steps, $h_{\max} = O(1/M)$, and we achieve the discretization error bound for DDIM algorithm:

$$\mathbf{x}_0 = \mathbf{x}_0^* + O(M(h_{\max}^2 + h_{\max}^2 L)) = \mathbf{x}_0^* + O(h_{\max} + h_{\max} L).$$

8.5 Proof for Proposition 4

Proof. By the definition of expectation, we have

$$\hat{f}(\mathbf{x}) = \mathbb{E}_{\epsilon \sim p(\epsilon)}[f(\mathbf{x} + \sigma_t \epsilon)] = (f \circledast p)(\mathbf{x}) = \int_{\mathbb{R}^n} f(\mathbf{z})p(\mathbf{x} - \mathbf{z})d\mathbf{z}.$$

Then we compute the Lipschitz constant

$$\mathbf{x}^T \nabla \hat{f}(\mathbf{x}) \leq C \int_{\mathbb{R}^n} \|\nabla p(\mathbf{x} - \mathbf{z})\|_2 d\mathbf{z} = C \int_{\mathbb{R}^n} \|\nabla p(\mathbf{z})\|_2 d\mathbf{z}.$$

As for the gradient Lipschitz constant, we have

$$L = \|\nabla^2 \hat{f}(\mathbf{x})\|_{\text{op}} \leq C \left\| \int_{\mathbb{R}^n} \nabla^2 p(\mathbf{x} - \mathbf{z}) d\mathbf{z} \right\|_{\text{op}} \leq C \int_{\mathbb{R}^n} \|\nabla^2 p(\mathbf{z})\|_{\text{op}} d\mathbf{z},$$

where $\|\cdot\|_{\text{op}}$ is the operator norm of a matrix.

8.6 Proof for Proposition 5

Our proof is based on the proof for Theorem 2 in [42]. The total error can be decomposed as the discrepancy between $q(\mathbf{x}_t^i)$ and $p_t(\mathbf{x}_t)$ and the error introduced by the ODE solver. We introduce an auxiliary process $q_t^r(\mathbf{y}_t^i)$, which initiates from the true distribution and perform the resampling steps. By triangle inequality:

$$\text{TV}(q_t(\mathbf{x}_t^i), p_t(\mathbf{x}_t)) \leq \text{TV}(q_t(\mathbf{x}_t^i), q_t^r(\mathbf{y}_t^i)) + \text{TV}(q_t^r(\mathbf{y}_t^i), p_t(\mathbf{x}_t)),$$

where the second term of RHS is bounded by $O(h_{\max})$ according to Proposition 3. Then we follow Lemma 1 in [42] to bound the first term.

$$\begin{aligned} &\mathbb{E}[\mathbf{1}[\mathbf{x}_t^{i+1} \neq \mathbf{y}_t^{i+1}]] \leq \mathbb{E}[\mathbf{1}[\mathbf{x}_{t+1}^{i+1} \neq \mathbf{y}_{t+1}^{i+1}]] \\ &\stackrel{(a)}{\leq} \mathbb{E} \left[\left(1 - Q \left(\frac{\sqrt{\beta_t} B}{2\sqrt{1 - \beta_t}} \right) \right) \mathbf{1}[\mathbf{x}_t^i \neq \mathbf{y}_t^i] \right] \\ &= \left(1 - Q \left(\frac{\sqrt{\beta_t} B}{2\sqrt{1 - \beta_t}} \right) \right) \mathbb{E}[\mathbf{1}[\mathbf{x}_t^i \neq \mathbf{y}_t^i]], \end{aligned}$$

where (a) uses Lemma 1 by setting $\mathbf{x}_{t+1}^{i+1} = \sqrt{\beta_t} \mathbf{x}_t^i + \sqrt{1-\beta_t} \mathbf{n}$ and $\mathbf{y}_{t+1}^{i+1} = \sqrt{\beta_t} \mathbf{y}_t^i + \sqrt{1-\beta_t} \mathbf{n}$. Applying the bound recursively, we have

$$\mathbb{E}[\mathbf{1}[\mathbf{x}_t^s \neq \mathbf{y}_t^s]] \leq \left(1 - Q\left(\frac{\sqrt{\beta_t} B}{2\sqrt{1-\beta_t}}\right)\right)^{s-1} \mathbb{E}[\mathbf{1}[\mathbf{x}_t^1 \neq \mathbf{y}_t^1]].$$

The conclusion follows by $\text{TV}(q_t(\mathbf{x}_t^i), q_t^r(\mathbf{y}_t^i)) \leq \mathbb{P}(\mathbf{x}_t^s \neq \mathbf{y}_t^s) = \mathbb{E}(\mathbf{1}[\mathbf{x}_t^s \neq \mathbf{y}_t^s])$ and the initial coupling $\text{TV}(q_t(\mathbf{x}_t^1), q_t^r(\mathbf{y}_t^1)) = \mathbb{P}(\mathbf{x}_t^1 \neq \mathbf{y}_t^1)$. Therefore, we conclude that

$$\begin{aligned} \text{TV}(q_t(\mathbf{x}_t^i), p_t(\mathbf{x}_t)) &\leq \text{TV}(q_t(\mathbf{x}_t^i), q_t^r(\mathbf{y}_t^i)) + \text{TV}(q_t^r(\mathbf{y}_t^i), p_t(\mathbf{x}_t)) \\ &\leq \left(1 - Q\left(\frac{\sqrt{\beta_t} B}{2\sqrt{1-\beta_t}}\right)\right)^{s-1} \text{TV}(q_t(\mathbf{x}_t^1), q_t^r(\mathbf{y}_t^1)) + O(h_{\max}) \\ &\leq \left(1 - Q\left(\frac{\sqrt{\beta_t} B}{2\sqrt{1-\beta_t}}\right)\right)^{s-1} \text{TV}(q_t(\mathbf{x}_t^1), p_t(\mathbf{x}_t)) + O(h_{\max}) + O(h_{\max}). \end{aligned}$$